Phytomedicine 124 (2024) 155289

Contents lists available at ScienceDirect

Phytomedicine

journal homepage: www.elsevier.com/locate/phymed

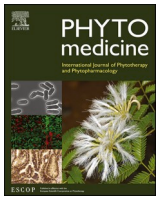

Original Article

Ginsenoside Rg3 promotes hepatic stellate cell ferroptosis by epigenetically regulating ACSL4 to suppress liver fibrosis progression

Yuhang Hu [a,b], Zhichao Lang [a], Xinmiao Li [a], Lifan Lin [a], Yifei Li [a], Rongrong Zhang [a], Jianjian Zheng [a,*], Zhengping Yu [c,*]

[a] Key Laboratory of Clinical Laboratory Diagnosis and Translational Research of Zhejiang Province, The First Affiliated Hospital of Wenzhou Medical University, No.2 Fuxue Lane, Wenzhou 325000, Zhejiang, PR China
[b] Cixi Biomedical Research Institute, Wenzhou Medical University, Ningbo 315300, Zhejiang, PR China
[c] Department of Hepatobiliary Surgery, The First Affiliated Hospital of Wenzhou Medical University, No.2 Fuxue Lane, Wenzhou 325000, Zhejiang, PR China

ARTICLE INFO

Keywords:
Ginsenoside Rg3
Ferroptosis
Methylation
MiR-6945–3p
HSC activation

ABSTRACT

Background: Ginsenoside Rg3 (G-Rg3), extracted from *Panax notoginseng*, possesses hepatoprotective properties. Hepatic stellate cells (HSCs) activation is responsible for liver fibrosis. Recent studies have reported the suppressive effects of G-Rg3 on HSC activation and proliferation. Ferroptosis is a novel iron regulated cell death. ACSL4, a key indicator of ferroptosis, is commonly methylated in various diseases.

Purpose: However, the role of ACSL4 methylation-mediated HSC ferroptosis in G-Rg3 inhibition of hepatic fibrosis needs to be explored.

Methods: Effects of G-Rg3 on inhibiting fibrosis were evaluated *in vivo* and *in vitro*. The impact of G-Rg3 on HSC ferroptosis was assessed *in vitro*. Furthermore, the expression of ACSL4, ACSL4 methylation and microRNA-6945–3p (miR-6945–3p) levels were determined.

Results: G-Rg3 significantly alleviated CCl_4-induced liver fibrosis, accompanied by collagen downregulation. *In vitro*, G-Rg3 contributed to HSC inactivation, leading to decreased collagen production. G-Rg3 induced HSC ferroptosis, characterized by increased iron accumulation, depletion of glutathione, malondialdehyde levels, and generation of lipid reactive oxygen species. Moreover, G-Rg3 promoted ACSL4 demethylation and restored its expression. Notably, DNMT3B counteracted the effect of G-Rg3-mediated inhibition of ACSL4 methylation and was targeted by miR-6945–3p. Further investigations revealed that G-Rg3 suppressed ACSL4 methylation through miR-6945–3p-mediated DNMT3B inhibition. Consistent with this, miR-6945–3p inhibition reversed G-Rg3-induced ACSL4 expression and HSC ferroptosis.

Conclusion: G-Rg3 inhibits ACSL4 methylation by miR-6945–3p-mediated DNMT3B inhibition, thereby promoting HSC ferroptosis and mitigating liver fibrosis.

Introduction

As a chronic and variable inflammatory liver disease (Yi et al., 2021), liver fibrosis occurs with an increase in the extracellular matrix (ECM) (Parola and Pinzani, 2019). It is an increasingly serious health issue, occurring in liver diseases (Kumar et al., 2021; Yue et al., 2021). Without intervention, liver fibrosis is more likely to deteriorate cirrhosis, liver dysfunction, and eventually hepatocellular carcinoma (Chen et al., 2022a). Activation of hepatic stellate cell (HSC) results in ECM production and excessive collagen deposition, driving liver fibrosis (El-Agroudy et al., 2016). Suppression of HSC activation may offer a potential approach for alleviating fibrosis (Bataller and Brenner, 2005).

MicroRNAs (miRNAs), endogenous non-coding RNAs (18–25nt), contribute to the regulation of basic biological processes (Ding et al.,

Abbreviation: ALT, alanine aminotransferase; CCl_4, carbon tetrachloride; Cont, control; Cur, Curcumin; DNMT3B-Mut, DNMT3B mutated type; DNMT3B-Wt, DNMT3B wild type; EC, esophageal carcinoma; ECM, extracellular matrix; G-Rg3, Ginsenoside Rg3; HA, hyaluronic acid; HSCs, Hepatic stellate cells; IHC, immunohistochemistry; MDA, malondialdehyde; miR-6945–3p, microRNA-6945–3p; miR-NC, miRNA-negative control; miRNAs, microRNAs; NASH, nonalcoholic steatohepatitis; Z-VAD, Z-VAD-FMK; 3′ UTR, 3′ untranslated region; α-SMA, alpha-smooth muscle actin; CCK-8, Cell Counting Kit-8; Col1A1, collagen type I alpha 1 chain; nec-1, necrostatin-1; qRT-PCR, quantitative real-time PCR; ROS, reactive oxygen species; GSH, glutathione.

* Corresponding authors.
E-mail addresses: zjj@wmu.edu.cn (J. Zheng), yuzhengping@wzhospital.cn (Z. Yu).

https://doi.org/10.1016/j.phymed.2023.155289
Received 7 September 2023; Received in revised form 21 November 2023; Accepted 15 December 2023
Available online 16 December 2023
0944-7113/© 2023 Elsevier GmbH. All rights reserved.

2022). MiRNAs exert their effects via mRNA 3′ untranslated region, thereby suppressing translation or promoting mRNA degradation (Cui et al., 2017; Hayes et al., 2014). Previous research has proved the essential impact of miRNAs on many diseases (Zhang et al., 2019). For example, miR-129–2–3p prohibits the growth of esophageal carcinoma (EC) cells, impeding EC development (Peng et al., 2023). MiR-690 has been shown to inhibit fibrogenesis and restore function of Kupffer cells in nonalcoholic steatohepatitis (NASH) (Gao et al., 2022). Notably, miRNAs are known to modulate HSC activation (Wu et al., 2018b). Additionally, Pinostilbene hydrate inhibits HSC activation via regulation of miR-17–5p and Wnt/β-catenin pathway (Zhou et al., 2020).

Ferroptosis, as a newly recognized type of cell death, is associated with diverse diseases (Stockwell et al., 2017). Yuan et al. (2022) demonstrated that sorafenib induces ferroptosis in HSCs to reduce liver injury and fibrosis. Thus, targeting ferroptotic death in HSCs represents a promising strategy to relieve liver fibrosis. Furthermore, Luo et al. elucidated that celastrol promotes ferroptosis in activated HSCs (Luo et al., 2022). ACSL4 participates in fatty acid conversion to fatty acyl-CoA esters, promoting ferroptosis by regulating lipid biosynthesis (Miao et al., 2022). ACSL4 expression is associated with its methylation status, and recent evidence indicates the downregulation of ACSL4 in liver diseases (Wang et al., 2022). Moreover, hypomethylated ACSL4 has been found in patients with NASH (Wu et al., 2018a).

Ginsenoside Rg3 (G-Rg3), a traditional Chinese herb, has been treated with human diseases owing to anti-inflammatory, anti-cancer, and hepatoprotective effects (Li et al., 2020b; Xia et al., 2022). G-Rg3 inhibits HSC autophagy by activating PI3K/Akt pathway, thereby suppressing inflammation and liver fibrosis (Liu et al., 2020). This study aimed to investigate whether ACSL4 methylation-mediated HSC ferroptosis is responsible for the inhibition of G-Rg3 on liver fibrosis.

Materials and methods

Study approval and mice treatment

C57BL/6 mice were treated with Carbon tetrachloride (CCl_4) (7 μl/g 10%; twice per week) for 8 weeks by intraperitoneal injection. The control (cont) group received the identical volume of olive oil. Two dose of G-Rg3 groups were gavaged G-Rg3 (10 or 20mg/kg) and the Curcumin (Cur) group was gavaged Cur (200mg/kg) everyday during CCl_4 treatment, respectively. Animal experiments were processed following guidelines of the local Animal Ethics Committee (wydw2023–0371, 2023–7–2).

Liver function assay

Serum alanine aminotransferase (ALT) as well as hyaluronic acid (HA) was detected by relative assay kits (Sinopharm Chemical Reagent).

Content of hydroxyproline in vivo

Homogenized liver tissues were hydrolyzed and evaporated. After corresponding reagent treatment, hydroxyproline content was quantified using hydroxyproline assay kits (Nanjing Jiancheng Bioengineering Institute).

Pathological examination and immunohistochemistry (IHC)

Collagen deposition levels were detected using Masson's trichrome, Sirius red staining and IHC as previously described (Lang et al., 2023).

Cell culture

Primary HSCs were isolated from mouse liver (Cho et al., 2010), and then cultured followed by past study (Chang et al., 2014). Primary HSCs were exposed to G-Rg3, Cur, ferrostain-1 (Fer-1), Z-VAD-FMK (Z-VAD), Necrostatin-1 (nec-1) or 5-Aza-2′-deoxycytidine (5-Aza) for 24h.

Analysis of cell counting Kit-8 (CCK-8)

10 μl CCK-8 reagent (YEASEN) was added in G-Rg3-treated cells for 1h. The absorbance was measured at 450nm.

Analysiss of 5-ethynyl-2′-deoxyuridine (EdU) assay

Cells were treated with G-Rg3 (20μM or 40μM) and Cur (80μM) and then incubated with EdU (Beyotime). After fixation and washing, cells reacted with Apollo reaction mixture.

Quantitative real-time PCR (qRT-PCR)

After extracted, RNA was reverse to cDNA using Reverse transcription kit (Promega). RT-PCR was performed via SYBR Green real-time PCR Master Mix. TaqMan MicroRNA Assays (Applied Biosystems) were used to examine miRNAs expressions. Data were normalized using β-actin or U6 (Applied Biological system). Primer sequences were shown in Table S1.

Western blot analysis

In brief, SDS-PAGE separated proteins, followed by electron transferring protein in gels onto PVDF membranes (Millipore, USA). Adding specific primary antibodies to membranes at 4℃ overnight. Subsequently, 1h of incubation with the secondary antibody was processed. Primary antibodies against α-SMA, ACSL4, GPX4, SLC7A11, DNMT1, DNMT3A, DNMT3B, type I collagen and β-actin (internal control) were purchased from Abcam (Cambridge, MA).

Transmission electron microscopy (TEM)

Primary HSCs were isolated from mice with G-Rg3 treatment. Cells were fixed with osmium acid and dehydrated by alcohol. Finally, images were captured by TEM after embedding with epoxy resin, cutting into ultrathin sections and staining.

Cell transfection

Primary HSCs were transfected with si-ACSL4 (50nM) and DNMT3B cDNA (3μg) using Lipofectamine RNAiMAX.

Methylation analysis

UCSC Genome Browser displayed CpG islands of ACSL4. The ACSL4 primers 5′-ATTTTGTTTAGTATTGTGGGAGTGG-3′ and 5′- AATCACAAACAACCTCTAACTCAAC-3′, were used to PCR analysis. The degree of ACSL4 methylation was evaluated as described previously (Veland et al., 2017).

Luciferase reporter assay

Co-transfection of miRNAs and pmirGLO-DNMT into HEK293T cells was performed using Lipofectamine RNAiMAX (Yu et al., 2020). Standardize the relative luciferase activity after transfection.

Detection of iron, lipid reactive oxygen species (ROS), malondialdehyde (MDA), and glutathione (GSH)

Assay kits were used to assess expressions of iron, lipid ROS, MDA, and GSH, as previously described (Yi et al., 2021).

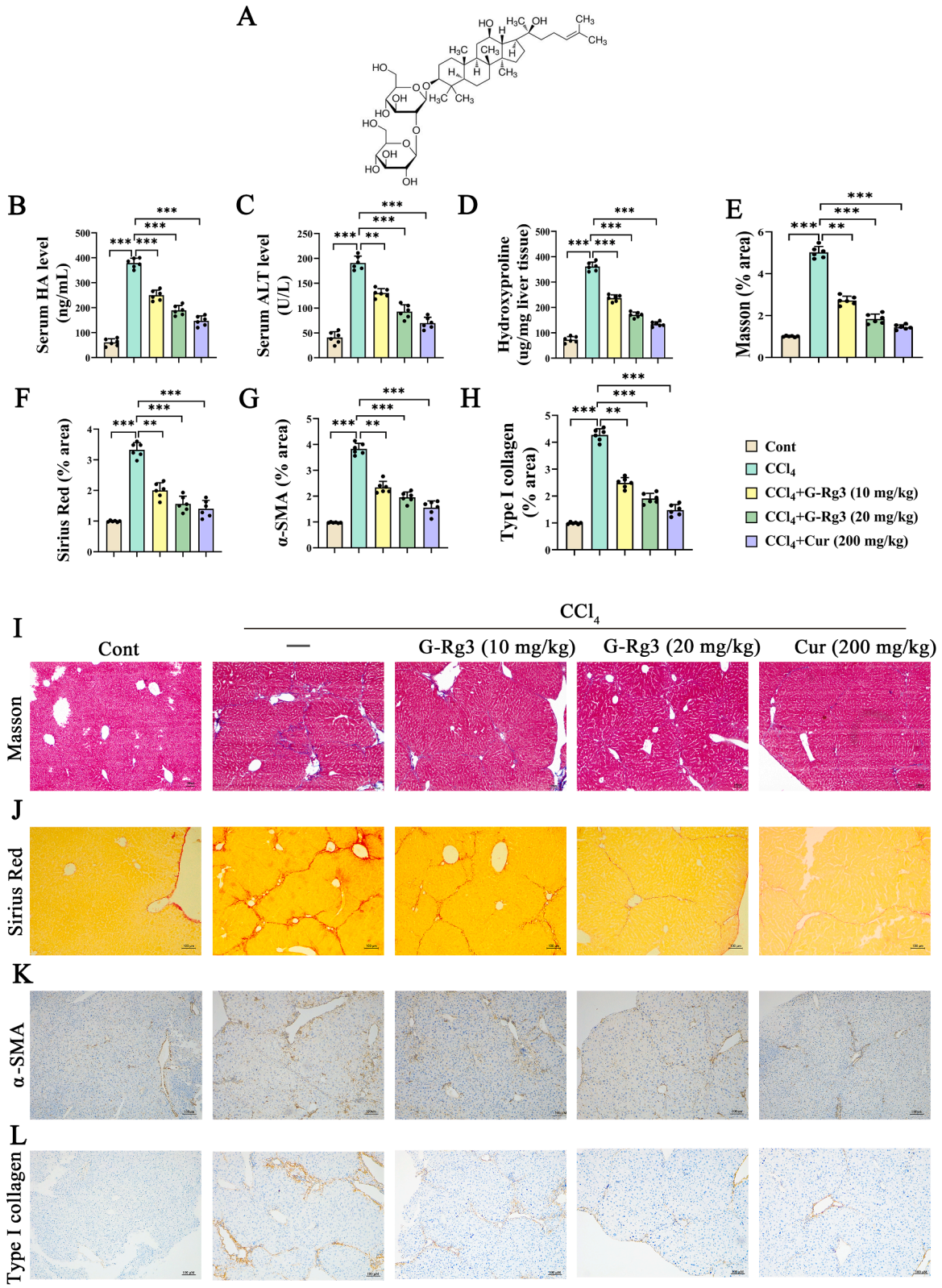

Fig. 1. G-Rg3 attenuates liver fibrosis development in the CCl_4 mouse model.
CCl_4 group recieved G-Rg3 (10 or 20mg/kg) or Cur (200mg/kg). Chemical structure of G-Rg3 (A). Analysis of HA (B), ALT (C), and hydroxyproline (D) levels in CCl_4 group after G-Rg3 treatment. The quantitative results of Masson (E), Sirius red (F), α-SMA (G), and type I collagen (H) staining. Collagen was examined by Masson (I) and Sirius red (J) staining. IHC of α-SMA (K) and type I collagen (L). Scale Bar (I-L), 100μm. $^{**}p < 0.01$ and $^{***}p < 0.001$.

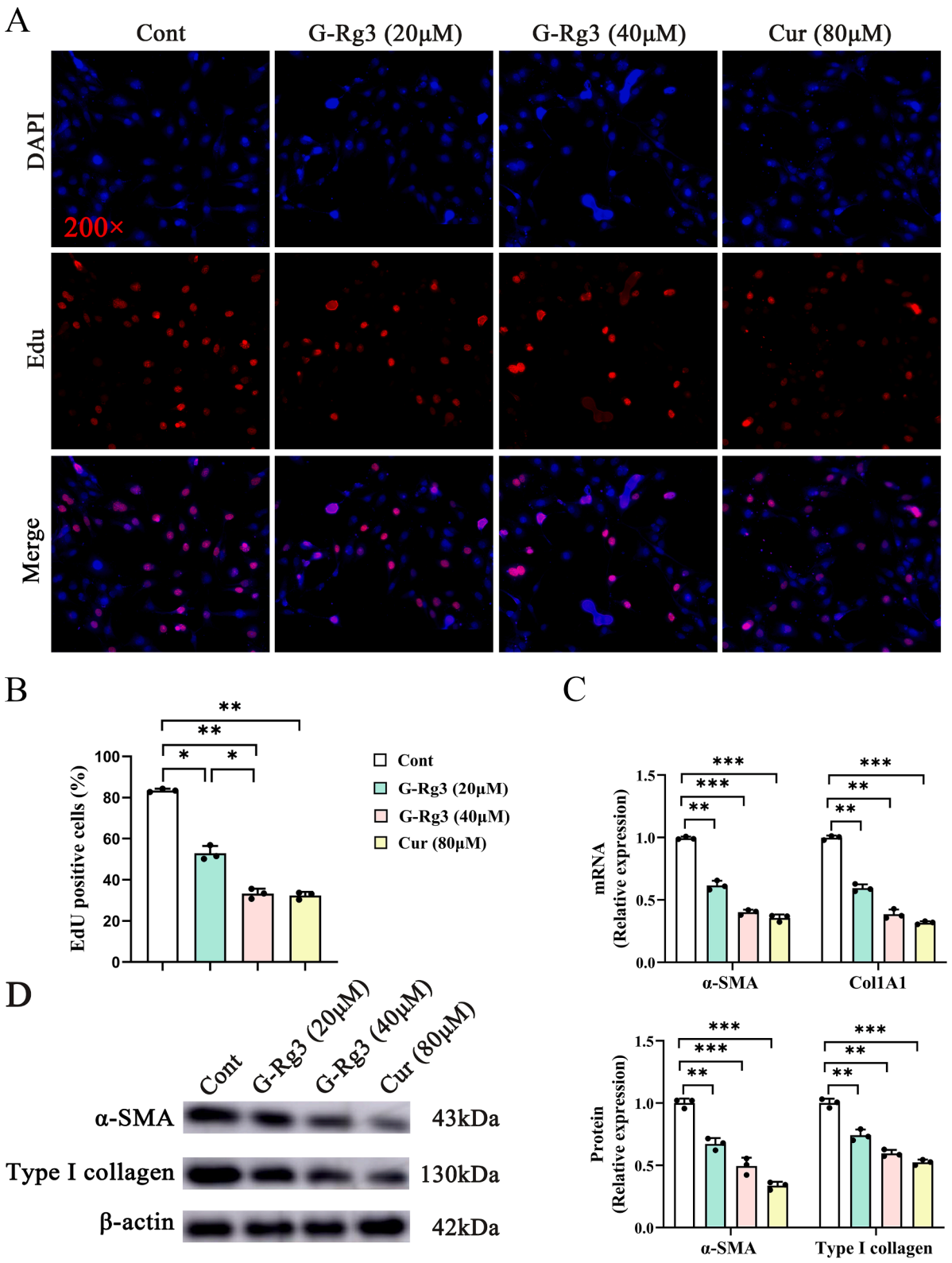

Fig. 2. G-Rg3 suppresses HSC activation *in vitro*.
HSCs were exposed to different concentrations of G-Rg3 (20 or 40μM) or Cur (80μM) for 24h. EdU assay (A and B). Relative mRNA (C), and protein (D) expressions of two major HSC activation markers α-SMA and Col1A1. *$p < 0.05$, **$p < 0.01$ and ***$p < 0.001$.

Statistical analysis

Data were represented as mean ± SD. Student's *t*-test was used to differentiate two groups and the One-way analysis of variance was applied to compare multiple groups. $p < 0.05$ was considered as significance.

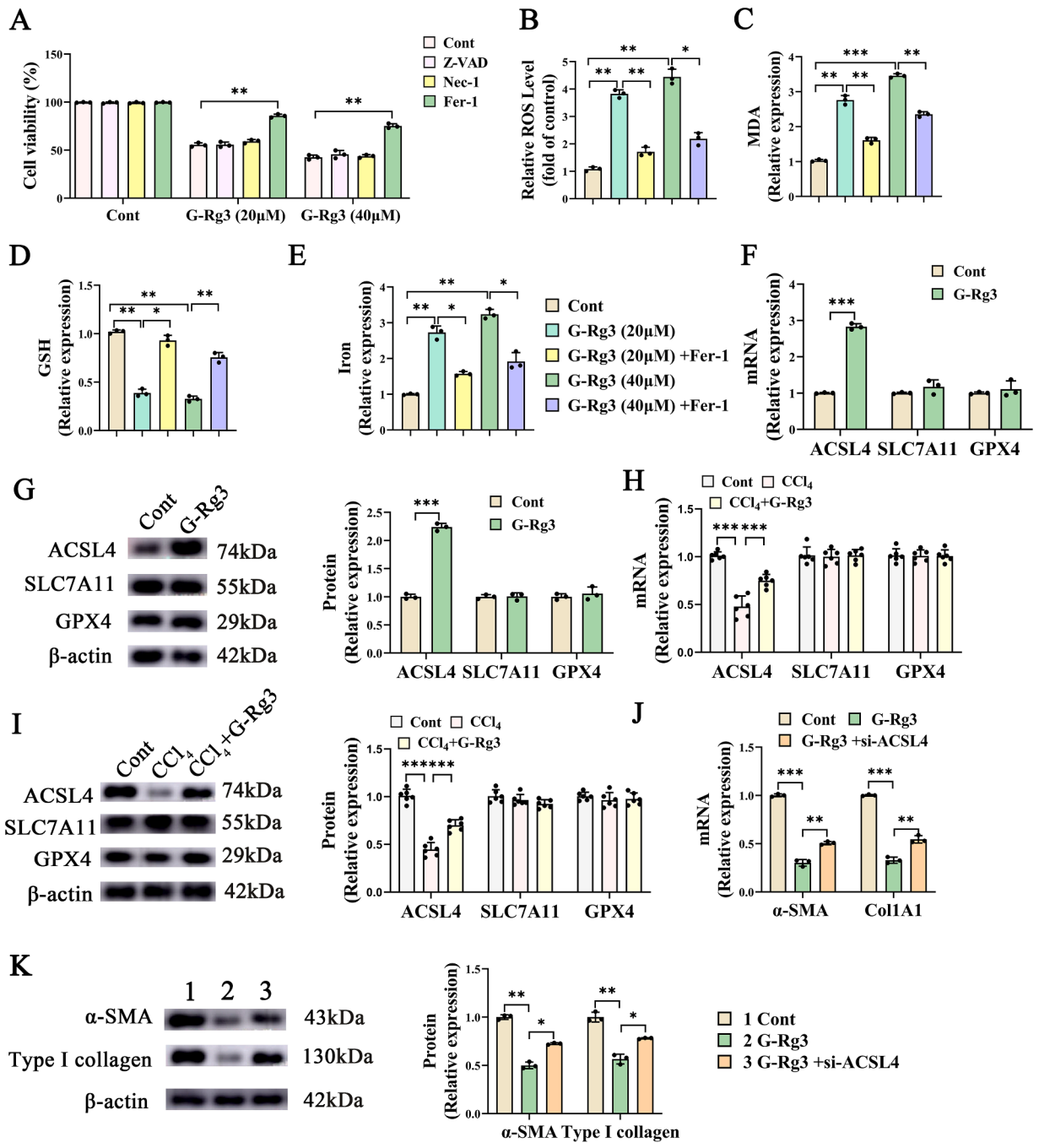

Fig. 3. G-Rg3 inhibits HSC activation through ACSL4-mediated HSC ferroptosis.
HSCs were treated with G-Rg3 (20, 40μM) with or without three cell death inhibitors (Fer-1, 1μM; Z-VAD, 10μM; nec-1, 10μM) for 24h. Cell viability was assessed by CCK-8 (A). ROS generation (B), MDA production (C), GSH depletion (D), and cellular iron (E) content in HSCs. Relative mRNA and protein levels of three ferroptosis regulators ACSL4, SLC7A11, and GPX4 in HSCs after G-Rg3 (40μM) treatment (F and G). Relative mRNA and protein levels of ACSL4, SLC7A11, and GPX4 in primary HSCs isolated from CCl_4-treated mice after G-Rg3 (20mg/kg) treatment (H and I). Relative mRNA, (J) and protein (K) levels of α-SMA and Col1A1 in HSCs after G-Rg3 (40μM) and si-ACSL4 (50nM) treatment. $^*p < 0.05$, $^{**}p < 0.01$, and $^{***}p < 0.001$.

Results

G-Rg3 attenuates liver fibrosis development in the CCl_4 mouse model

Excessive collagen deposition is a hallmark of liver fibrosis (Zhang et al., 2016), and CCl_4 is commonly used to induce liver fibrosis (Geng et al., 2020). As shown in Fig. 1B–D, CCl_4-treated mice showed high levels of HA, ALT, and hydroxyproline compared to the cont group, indicating liver injury induced by CCl_4 treatment. Treatment with G-Rg3 resulted in reduced HA and ALT levels in CCl_4-treated mice (Fig. 1B and C), indicating the amelioration of liver injury by G-Rg3. Moreover, G-Rg3 significantly inhibited hydroxyproline elevation induced by CCl_4 (Fig. 1D). As a positive control, Cur reduced CCl_4-induced HA, ALT, and hydroxyproline (Fig. 1B–D). Masson staining and Sirius staining demonstrated that the increased collagen levels induced by CCl_4 were suppressed by G-Rg3 (Fig. 1E, F, I and J). Consistently, G-Rg3 inhibited CCl_4-induced liver fibrosis, as evidenced by decreased α-SMA and collagen (Fig. 1G, H, K and L). Similar anti-fibrosis effects were observed in CCl_4-treated mice after Cur treatment (Fig. 1E–L). Collectively, these findings provide evidence that G-Rg3 alleviates CCl_4-induced liver

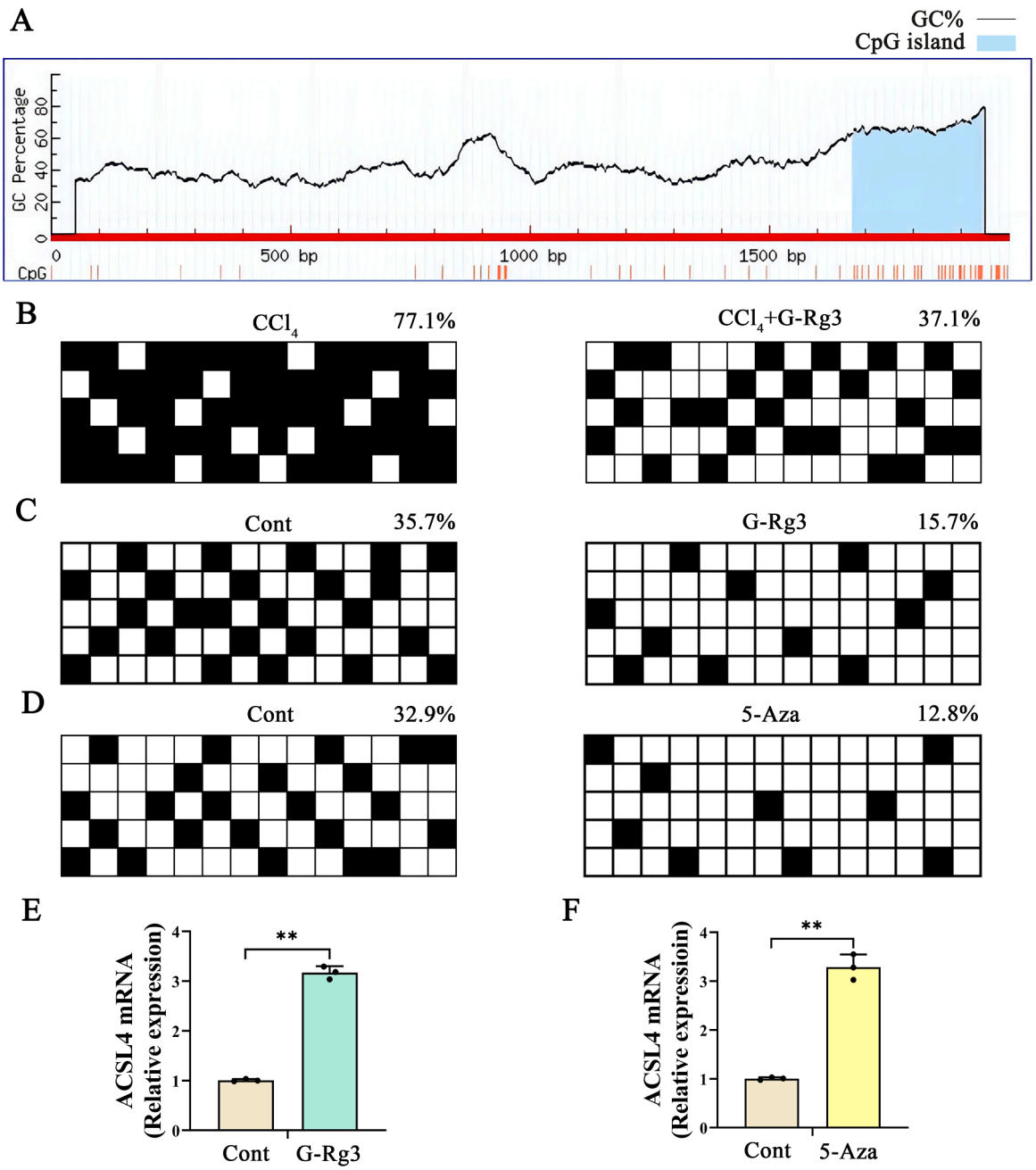

Fig. 4. Enhanced ACSL4 expression is associated with its demethylation status.
Sketch map displayed the CpG island of ACSL4. CpG dinucleotides were shown by vertical lines (A). Levels of ACSL4 methylation in primary HSCs isolated from CCl_4 group following G-Rg3 (20mg/kg) treatment (B), G-Rg3 (40μM)-treated HSCs (C), and 5-Aza (2.5μM)-treated HSCs (D). The results of PCR products were demonstrated through squares to use monoclonal sequential analysis. Black and white squares showed methylated CpG locus and unmethylated locus, respectively. Relative mRNA levels of ACSL4 in HSCs after G-Rg3 (E) and 5-Aza (F) treatment. $^{**}p < 0.01$.

fibrosis.

G-Rg3 suppresses HSC activation in vitro

HSC activation, characterized by enhanced cell proliferation, leads to ECM production during liver fibrosis (Yu et al., 2018). Effect of G-Rg3 on HSC proliferation was subsequently examined. EdU analysis indicated that G-Rg3 suppressed HSC proliferation in a dose-dependent manner (Fig. 2A and B). G-Rg3 treatment also decreased expressions of α-SMA and collagen type I alpha 1 chain (Col1A1), indicating its inhibitory effect on HSC activation (Fig. 2C and D). Similar results, including reduced cell proliferation, α-SMA and Col1A1 expression, were observed in Cur-treated cells (Fig. 2C and D). Therefore, G-Rg3 suppresses the activation of HSC *in vitro*.

G-Rg3 inhibits HSC activation through ACSL4-mediated HSC ferroptosis

Regulated cell death mechanisms consist of ferroptosis, apoptosis, and necroptosis, which are associated with liver fibrosis (Huang et al., 2022; Li et al., 2020a, 2022). Therefore, we employed the ferroptosis inhibitor Fer-1, apoptosis inhibitor Z-VAD, and necroptosis inhibitor nec-1 in G-Rg3-treated cells. Our results revealed that the viability of HSC inhibited by G-Rg3 was only restored by Fer-1, indicating that ferroptosis is involved in the effects of G-Rg3 on HSC death (Fig. 3A).

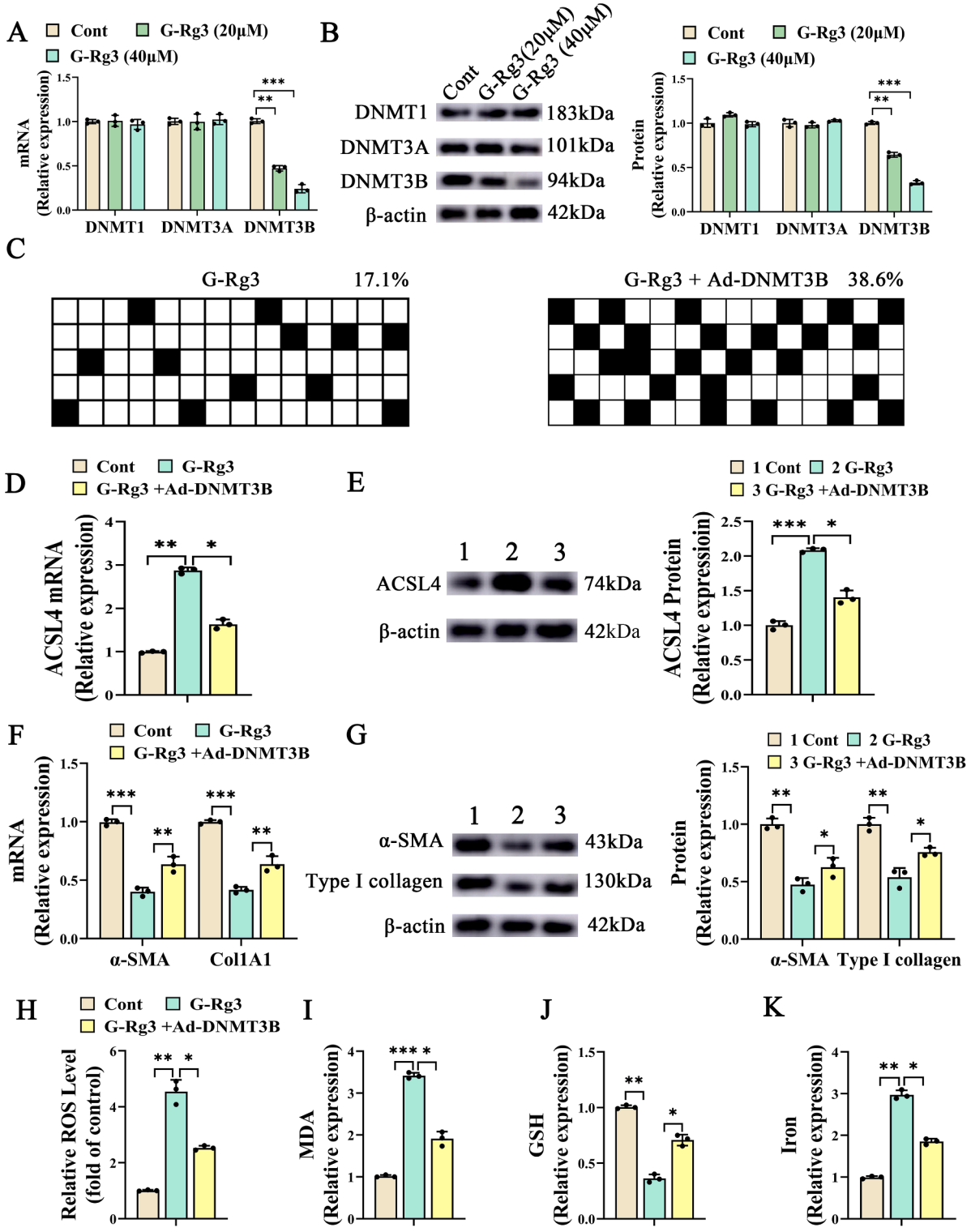

Fig. 5. ACSL4 methylation is mediated by DNMT3B.
Relative mRNA (A) and protein (B) levels of DNMT1, DNMT3A, and DNMT3B in HSCs after G-Rg3 (20μM or 40μM). Levels of ACSL4 methylation in HSCs after G-Rg3 (40μM) treatment with or without Ad-DNMT3B (C). Relative mRNA (D) and protein (E) levels of ACSL4 in HSCs. Relative mRNA (F) and protein (G) levels of α-SMA and Col1A1 in HSCs. ROS generation (H), MDA production (I), GSH depletion (J), and cellular iron (K) content of HSCs. $^{*}p < 0.05$, $^{**}p < 0.01$, and $^{***}p < 0.001$.

ROS generation, MDA production, GSH depletion and redox-active iron accumulation, as key events of ferroptosis, were elevated by G-Rg3 (Fig. 3B–E). Importantly, Fer-1 reversed the G-Rg3-mediated effects on ferroptosis (Fig. 3B–E). Moreover, in isolated primary HSCs, TEM analysis showed that G-Rg3 enhanced mitochondrial cristae disappearance in comparison with the CCl_4 group (Fig. S1). Likewise, G-Rg3 led to an increase in MDA production and GSH depletion in primary HSCs, which further confirmed the role of G-Rg3 in HSC ferroptosis (Fig. S2). Together, these results confirmed that G-Rg3 induces HSC ferroptosis. ACSL4, SLC7A11, and GPX4 are well-known

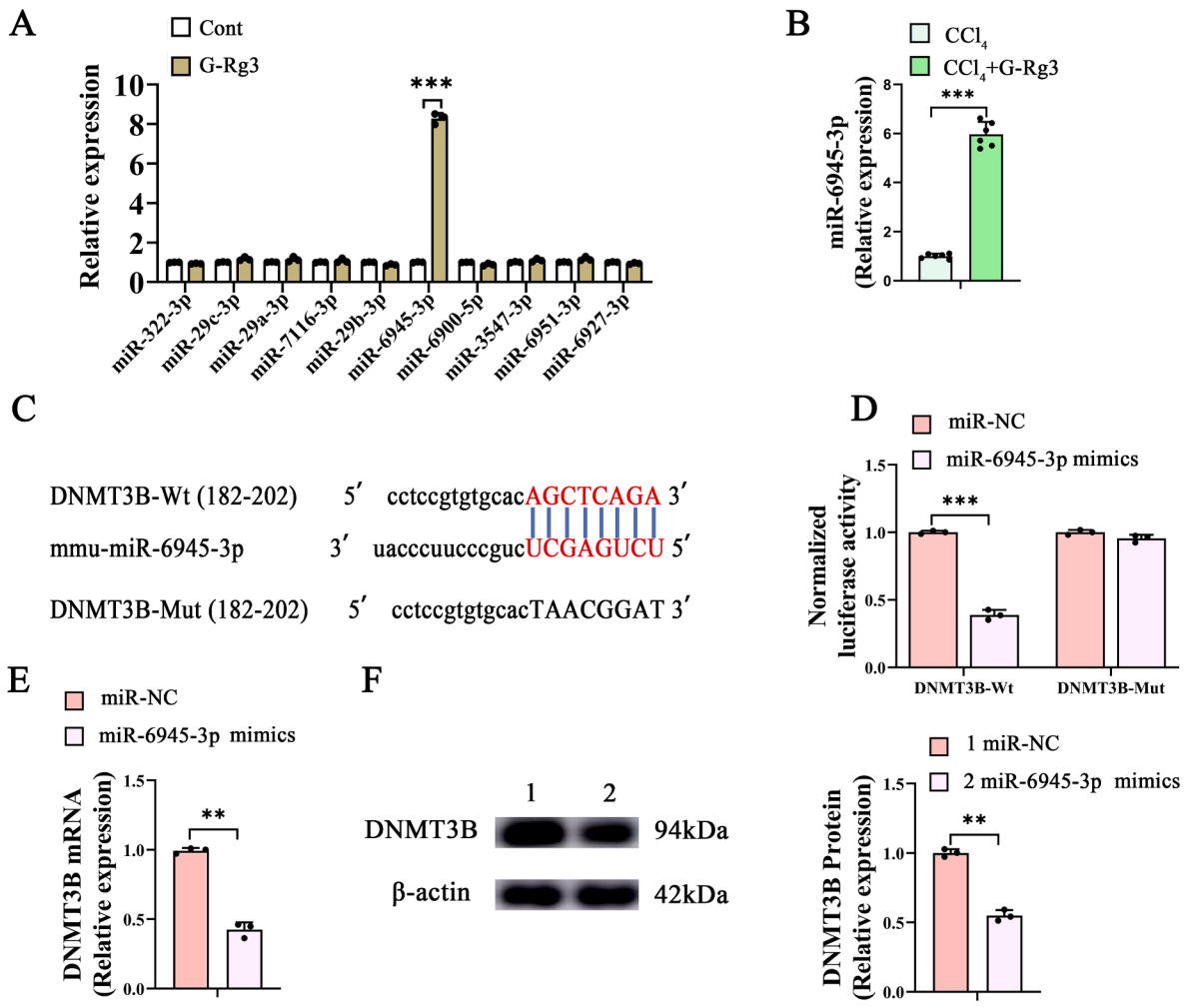

Fig. 6. DNMT3B is a miR-6945–3p target.
Expressions of predicted miRNAs in HSCs after G-Rg3 (40μM) treatment (A). miR-6945–3p expression in primary HSCs isolated from CCl_4-treated mice after G-Rg3 (20mg/kg) treatment (B). miR-6945–3p-binding sites in the 3′-UTR of DNMT3B mRNA (C). Relative luciferase activity (D). Relative mRNA (E) and protein (F) levels of DNMT3B in HSCs after miR-6945–3p mimic transfection. $^{**}p < 0.01$ and $^{***}p < 0.001$.

ferroptosis-related genes (Luo et al., 2021; Wang et al., 2019), but G-Rg3 treatment specifically upregulated ACSL4 expression without affecting SLC7A11 or GPX4 levels in HSCs (Fig. 3F and G) and in CCl_4-treated mice (Fig. 3H and I). Silencing ACSL4 restored the G-Rg3-induced reduction in α-SMA and Col1A1 expression in HSCs (Fig. 3J and K). Collectively, our findings suggest that G-Rg3 suppresses HSC activation through ACSL4-mediated HSC ferroptosis.

Enhanced ACSL4 expression is associated with its demethylation status

Growing evidence supports the association between ACSL4 expression and its methylation status. Bioinformatics analysis revealed a CpG island in the ACSL4 promoter with 14 CpG sites (Fig. 4A). The average methylation frequency of ACSL4 in CCl_4-treated mice was 77.1%, which significantly decreased to 37.1% after G-Rg3 treatment (Fig. 4B). Moreover, G-Rg3 treatment also suppressed ACSL4 methylation in HSCs (Fig. 4C). Consistent with these findings, mRNA expression of ACSL4 was elevated after G-Rg3 treatment (Fig. 4E). To further investigate the role of DNA methylation, we treated HSCs with 5-Aza, a DNMT inhibitor. The treatment resulted in reduced ACSL4 methylation and increased expression (Fig. 4D and F). Together, these findings reveal that ACSL4 expression is related to its demethylation status in G-Rg3-treated HSCs.

ACSL4 methylation is mediated by DNMT3B

DNMTs, key regulators of DNA methylation, demonstrate vital roles in various diseases development. The DNMTs family comprises three major members: DNMT1, DNMT3A, and DNMT3B (Bai et al., 2022; Leonard et al., 2011). Teng et al. (2017) reported that G-Rg3 downregulates DNMT3B in HepG2 cells. To explore whether DNMTs are involved in ACSL4 methylation, we examined the expressions of DNMT1, DNMT3A, and DNMT3B in G-Rg3-treated HSCs. qRT-PCR and western blot analyses revealed that only DNMT3B was downregulated by G-Rg3 in HSCs (Fig. 5A and B). Also, G-Rg3 resulted in a reduction in DNMT3B in CCl_4-treated mice (Fig. S3). Subsequently, we investigated the role of DNMT3B in G-Rg3-mediated ACSL4 demethylation. DNMT3B overexpression reversed the effect of G-Rg3 on ACSL4 demethylation and expression (Fig. 5C–E). Furthermore, DNMT3B overexpression counteracted the suppression of G-Rg3 on HSC activation, as indicated by elevated levels of α-SMA and Col1A1 (Fig. 5F and G). We further explored whether ACSL4-mediated HSC ferroptosis is regulated by DNMT3B. Notably, DNMT3B inhibited G-Rg3-induced ferroptosis in HSCs, leading to reduced ROS generation, MDA production, GSH depletion and iron levels (Fig. 5H–K). In summary, these findings suggest that G-Rg3 promotes ACSL4 expression by inhibiting DNMT3B-mediated ACSL4 methylation.

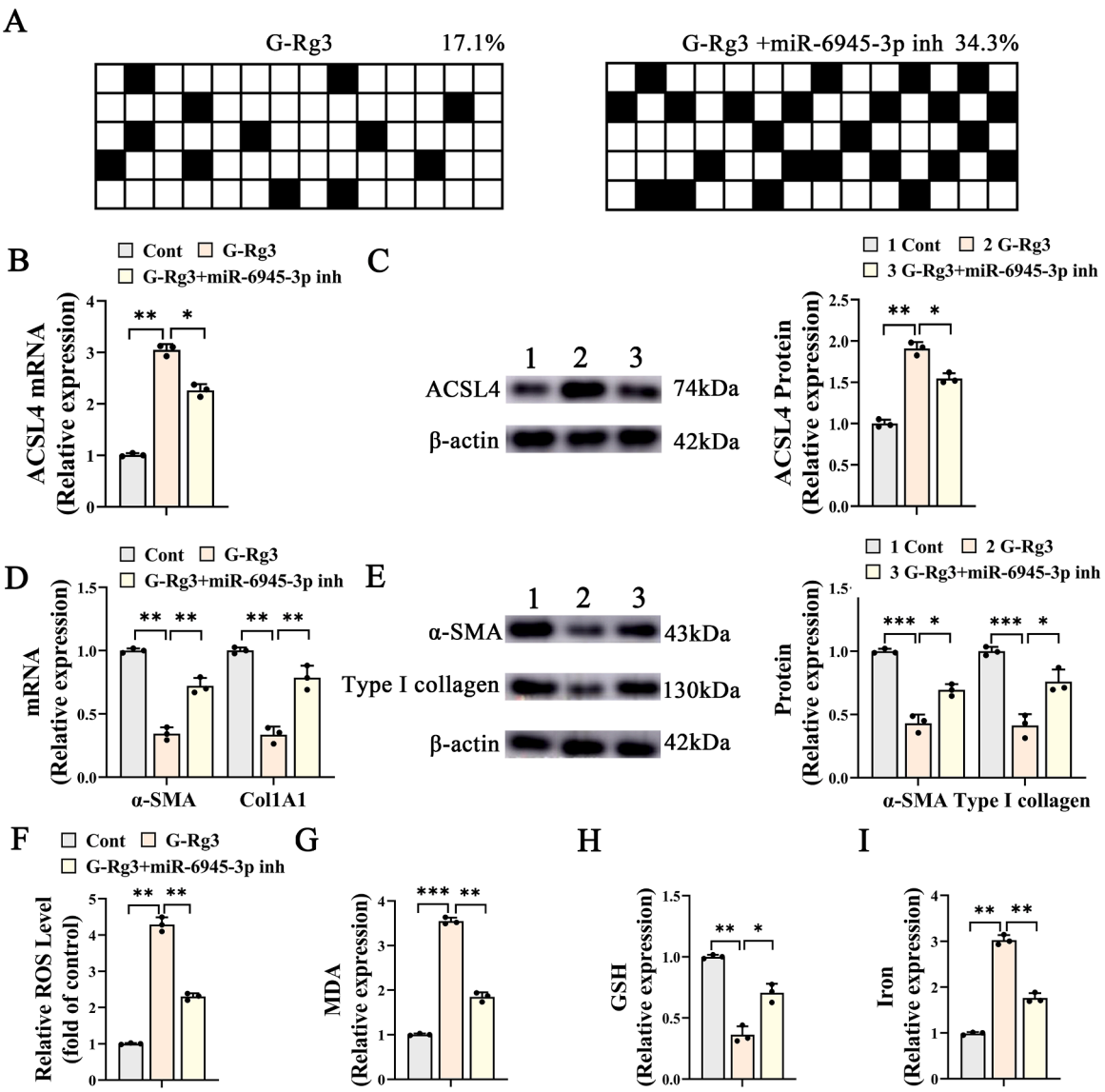

Fig. 7. MiR-6945–3p-mediated ACSL4 demethylation is involved in the effects of G-Rg3 on HSC ferroptosis.
HSCs were exposed to G-Rg3 (40μM) and miR-6945–3p inhibitor. The levels of ACSL4 methylation treated with G-Rg3 with or without miR-6945–3p inhibitor (A). Relative mRNA (B) and protein (C) levels of ACSL4. Relative mRNA (D) and protein (E) levels of α-SMA and Col1A1. ROS generation (F), MDA production (G), GSH depletion (H), and cellular iron (I) content of HSCs. $^{*}p < 0.05$, $^{**}p < 0.01$ and $^{***}p < 0.001$.

DNMT3B is a microRNA-6945–3p (MiR-6945–3p) target

MiRNAs exert a significant influence on the development of various diseases by targeting specific genes. For example, miRNA-mediated regulation of DNMT3B has been observed in different cancer types, including lung cancer (Hammell, 2010) and melanoma (Schoof et al., 2015). To explore potential miRNAs targeting DNMT3B, bioinformatics analysis was performed. Fig. 6A shows the prediction results from miRDB, identifying ten potential miRNAs, including miR-322–3p, miR-29c-3p, miR-29a-3p, miR-7116–3p, miR-29b-3p, miR-6945–3p, miR-6900–5p, miR-3547–3p, miR-6951–3p, and miR-6927–3p. Subsequently, we found that G-Rg3 specifically upregulated miR-6945–3p, while other miRNAs remained unchanged. *In vivo*, G-Rg3 treatment also led to an elevation in miR-6945–3p levels in CCl_4-induced mice (Fig. 6B). To confirm the interaction between miR-6945–3p and DNMT3B, luciferase reporters were constructed containing either DNMT3B wild-type (DNMT3B-Wt) or DNMT3B mutated (DNMT3B-Mut) binding site for miR-6945–3p (Fig. 6C). MiR-6945–3p significantly reduced luciferase activities of DNMT3B-Wt, but made no difference on DNMT3B-Mut (Fig. 6D). Therefore, we verified DNMT3B as a direct target of miR-6945–3p. Consistently, miR-6945–3p mimics decreased expressions of DNMT3B (Fig. 6E and F). These findings provide evidence that miR-6945–3p specifically targets DNMT3B.

MiR-6945–3p-mediated ACSL4 demethylation is involved in the effects of G-Rg3 on HSC ferroptosis

Finally, we investigated the role of miR-6945–3p in G-Rg3-induced ACSL4 demethylation. Cells treated with the miR-6945–3p inhibitor exhibited increased ACSL4 methylation compared to G-Rg3-treated cells alone (Fig. 7A). Moreover, the elevation of ACSL4 induced by G-Rg3 was attenuated by the miR-6945–3p inhibitor (Fig. 7B and C). Furthermore, miR-6945–3p inhibition reversed the inhibitory effect of G-Rg3 on HSC activation, accompanied by elevated α-SMA and type I collagen expression (Fig. 7D and E). Furthermore, G-Rg3-induced HSC ferroptosis was impeded by the miR-6945–3p inhibitor (Fig. 7F–I). Collectively, these findings demonstrate that G-Rg3 promotes HSC ferroptosis through miR-6945–3p-mediated ACSL4 demethylation.

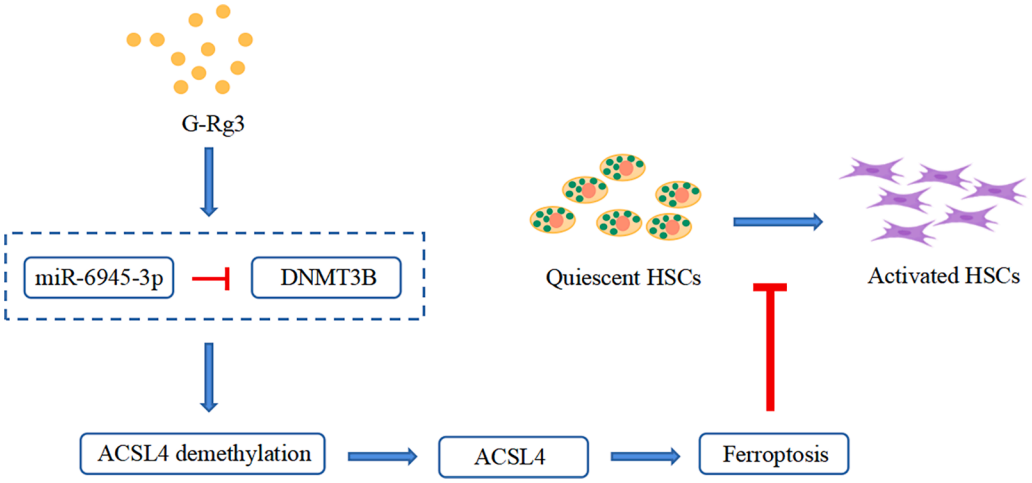

Fig. 8. Graphical diagram of the working model illustrating how G-Rg3 attenuates liver fibrosis by inducing HSC ferroptosis via miR-6945–3p/ACSL4 pathway.

Discussion

G-Rg3 is a well-known therapeutic agent for various hepatic diseases, including liver fibrosis and cancers. For example, G-Rg3 induces melanoma cell death by inhibiting FUT4 expression (Shan et al., 2015). A recent study found that G-Rg3 suppresses hepatic fibrosis development via inhibiting inflammation-mediated autophagy signaling pathway (Liu et al., 2020). Consistently, G-Rg3 exhibited an anti-fibrosis effect *in vivo*. G-Rg3 contributed to the inhibition of HSC activation, which was associated with enhanced HSC ferroptosis. Notably, G-Rg3 upregulated ACSL4, a promoter of HSC ferroptosis (Liao et al., 2022). Further studies indicated that G-Rg3-mediated ACSL4 demethylation was inhibited by miR-6945–3p inhibitor or DNMT3B overexpression. Furthermore, miR-6945–3p targeted DNMT3B. Taken together, this study reveals that G-Rg3 exerts a crucial effect on HSC ferroptosis, at least partially through epigenetic modulation of ACSL4, representing a novel therapeutic mechanism of G-Rg3 in liver fibrosis treatment (Fig. 8).

Ferroptosis is characterized by iron and ROS accumulation. Ferroptosis dysregulation has been shown to contribute to the development of cancers. Targeting ferroptosis-related pathways is a potential therapeutic strategy. Suppression of both NFS1 and cysteine cooperation transport triggers ferroptosis *in vitro* (Alvarez et al., 2017), leading to the inhibition of tumor growth (Cho et al., 2022). Recently, Zhang et al. demonstrated that artemether treatment effectively attenuates liver fibrosis and promotes HSC inactivation through the induction of p53-mediated HSC ferroptosis (Zhang et al., 2020). Consistent with these reports, our study revealed the involvement of ferroptosis in G-Rg3-mediated suppression of HSC activation, accompanied by increased ACSL4 expression and demethylation. ACSL4 upregulation is linked to ferroptosis in multiple diseases (Zhang et al., 2018), and our study demonstrated that G-Rg3 restored ACSL4 expression through demethylation in HSCs. In summary, our research shows that G-Rg3 promotes HSC ferroptosis and suppresses HSC activation by modulating ACSL4 expression, providing a novel insight into the therapeutic potential of G-Rg3 during liver fibrosis.

DNA methylation is an epigenetic mechanism, which regulates gene expression (Vrtačnik et al., 2015). Numerous studies demonstrate that DNA methylation is associated with diseases. For example, inhibiting DNMT and HDAC genes slows down cancer development and tumor metastasis (Zhang et al., 2022). Interestingly, DNMT3B, which is frequently up-regulated in cancers, has emerged with poor prognosis (Beetch et al., 2021). In our study, G-Rg3 specifically inhibited DNMT3B expression, while DNMT1 and DNMT3A remained unaffected. Overexpression of DNMT3B counteracted the demethylation of ACSL4 mediated by G-Rg3, resulting in reduced ACSL4 levels and the inhibition of HSC ferroptosis. Meanwhile, DNMT3B also blocked down G-Rg3-induced HSC inactivation. Collectively, our study indicates that DNMT3B-mediated ACSL4 methylation participates in the modulation of HSC ferroptosis and activation by G-Rg3.

MiRNAs is involved in regulating diseases, such as liver metabolism, liver fibrosis (Chen et al., 2022b), and tumor development (Wang et al., 2021). In the context of HSC activation, miRNAs play significant regulatory roles. For example, miR-29a regulates HSC activation by modulating the profibrogenic phenotype of HSC (Huang et al., 2018). In our study, we discovered that miR-6945–3p is a suppressor of liver fibrosis. MiR-6945–3p experssion was enhanced by G-Rg3. Subsequent experiments indicated that miR-6945–3p targets DNMT3B. Importantly, miR-6945–3p-mediated ACSL4 demethylation was involved in the effects of G-Rg3 on HSC inactivation. Moreover, inhibition of miR-6945–3p substantially attenuated the G-Rg3-induced increased ACSL4 expression and HSC ferroptosis. Collectively, our results suggest that G-Rg3 induces HSC ferroptosis through miR-6945–3p-mediated ACSL4 demethylation. However, the precise mechanisms underlying G-Rg3 regulation of miR-6945–3p require further investigation.

Conclusion

Our study provides evidence that G-Rg3 promotes the demethylation of ACSL4 and restores its expression through miR-6945–3p-mediated DNMT3B inhibition. This mechanism contributes to HSC ferroptosis and, consequently, the inhibition of liver fibrosis. The novel link between G-Rg3, ACSL4, and miR-6945–3p sheds new light on the potential role of G-Rg3 in HSC ferroptosis and liver fibrosis, offering insights into liver fibrosis treatment.

Funding statement

The project was supported by Zhejiang Provincial Medical and Health Planning Project (No.2023KY898), Zhejiang Provincial Research Centre for Diagnosis and Treatment of Critical Liver and Biliary Diseases (Minimally Invasive), National Clinical Key Specialty Project (General Surgery), and Wenzhou Municipal Science and technology Bureau (No. Y20220023).

CRediT authorship contribution statement

Yuhang Hu: Data curation, Formal analysis, Investigation, Methodology, Project administration, Resources, Software, Writing – original draft. **Zhichao Lang:** Data curation, Formal analysis, Investigation, Methodology, Project administration, Resources, Software, Writing –

original draft. **Xinmiao Li:** Data curation, Formal analysis, Writing – original draft. **Lifan Lin:** Data curation, Formal analysis, Writing – original draft. **Yifei Li:** Data curation, Formal analysis, Writing – original draft. **Rongrong Zhang:** Data curation, Formal analysis, Writing – original draft. **Jianjian Zheng:** Conceptualization, Supervision, Writing – review & editing. **Zhengping Yu:** Conceptualization, Supervision, Writing – review & editing.

Declaration of Competing Interest

We declare that we have no financial and personal relationships with other people or organizations that can inappropriately influence our work, there is no professional or other personal interest of any nature or kind in any product, service and/or company that could be construed as influencing the position presented in, or the review of, the manuscript entitled, "Ginsenoside Rg3 promotes hepatic stellate cell ferroptosis by epigenetically regulating ACSL4 to suppress liver fibrosis progression".

Supplementary materials

Supplementary material associated with this article can be found, in the online version, at doi:10.1016/j.phymed.2023.155289.

References

Alvarez, S.W., Sviderskiy, V.O., Terzi, E.M., Papagiannakopoulos, T., Moreira, A.L., Adams, S., Sabatini, D.M., Birsoy, K., Possemato, R., 2017. NFS1 undergoes positive selection in lung tumours and protects cells from ferroptosis. Nature 551, 639–643.

Bai, L., Hao, X., Keith, J., Feng, Y., 2022. DNA methylation in regulatory T cell differentiation and function: challenges and opportunities. Biomolecules 12.

Bataller, R., Brenner, D.A., 2005. Liver fibrosis. J. Clin. Invest. 115, 209–218.

Beetch, M., Boycott, C., Harandi-Zadeh, S., Yang, T., Martin, B.J.E., Dixon-McDougall, T., Ren, K., Gacad, A., Dupuis, J.H., Ullmer, M., Lubecka, K., Yada, R.Y., Brown, C.J., Howe, L.J., Stefanska, B., 2021. Pterostilbene leads to DNMT3B-mediated DNA methylation and silencing of OCT1-targeted oncogenes in breast cancer cells. J. Nutr. Biochem. 98, 108815.

Chang, W., Yang, M., Song, L., Shen, K., Wang, H., Gao, X., Li, M., Niu, W., Qin, X., 2014. Isolation and culture of hepatic stellate cells from mouse liver. Acta Biochim. Biophys. Sin. 46, 291–298. Shanghai.

Chen, H.J., Huang, J.Y., Ko, C.Y., 2022a. Peach kernel extracts inhibit lipopolysaccharide-induced activation of HSC-T6 hepatic stellate cells. Int. J. Clin. Pract. 2022, 4869973.

Chen, J., Li, X., Ge, C., Min, J., Wang, F., 2022b. The multifaceted role of ferroptosis in liver disease. Cell Death Differ. 29, 467–480.

Cho, I.J., Kim, Y.W., Han, C.Y., Kim, E.H., Anderson, R.A., Lee, Y.S., Lee, C.H., Hwang, S. J., Kim, S.G., 2010. E-cadherin antagonizes transforming growth factor β1 gene induction in hepatic stellate cells by inhibiting RhoA-dependent Smad3 phosphorylation. Hepatology 52, 2053–2064.

Cho, S.S., Yang, J.H., Lee, J.H., Baek, J.S., Ku, S.K., Cho, I.J., Kim, K.M., Ki, S.H., 2022. Ferroptosis contribute to hepatic stellate cell activation and liver fibrogenesis. Free Radic. Biol. Med. 193, 620–637.

Cui, J., Zhou, B., Ross, S.A., Zempleni, J., 2017. Nutrition, microRNAs, and human health. Adv. Nutr. 8, 105–112.

Ding, R., Hong, W., Huang, L., Shao, J., Yu, W., Xu, X., 2022. Examination of the effects of microRNA-145-5p and phosphoserine aminotransferase 1 in colon cancer. Bioengineered 13, 12794–12806.

El-Agroudy, N.N., El-Naga, R.N., El-Razeq, R.A., El-Demerdash, E., 2016. Forskolin, a hedgehog signalling inhibitor, attenuates carbon tetrachloride-induced liver fibrosis in rats. Br. J. Pharmacol. 173, 3248–3260.

Gao, H., Jin, Z., Bandyopadhyay, G., Cunha, E.R.K., Liu, X., Zhao, H., Zhang, D., Jouihan, H., Pourshahian, S., Kisseleva, T., Brenner, D.A., Ying, W., Olefsky, J.M., 2022. MiR-690 treatment causes decreased fibrosis and steatosis and restores specific Kupffer cell functions in NASH. Cell Metab. 34, 978–990 e974.

Gasque Schoof, C.R., Izzotti, A., Jasiulionis, M.G., Vasques Ldos, R., 2015. The roles of miR-26, miR-29, and miR-203 in the silencing of the epigenetic machinery during melanocyte transformation. Biomed. Res. Int. 2015, 634749.

Geng, W., Zhou, G., Zhao, B., Xiao, Q., Li, C., Fan, S., Dong, P., Zheng, J., 2020. Liquiritigenin suppresses the activation of hepatic stellate cells via targeting miR-181b/PTEN axis. Phytomedicine 66, 153108.

Hammell, M., 2010. Computational methods to identify miRNA targets. Semin. Cell Dev. Biol. 21, 738–744.

Hayes, J., Peruzzi, P.P., Lawler, S., 2014. MicroRNAs in cancer: biomarkers, functions and therapy. Trends Mol. Med. 20, 460–469.

Huang, S., Wang, Y., Xie, S., Lai, Y., Mo, C., Zeng, T., Kuang, S., Zhou, C., Zeng, Z., Chen, Y., Huang, S., Gao, L., Lv, Z., 2022. Isoliquiritigenin alleviates liver fibrosis through caveolin-1-mediated hepatic stellate cells ferroptosis in zebrafish and mice. Phytomedicine 101, 154117.

Huang, Y.H., Yang, Y.L., Wang, F.S., 2018. The role of miR-29a in the regulation, function, and signaling of liver fibrosis. Int. J. Mol. Sci. 19.

Kumar, S., Duan, Q., Wu, R., Harris, E.N., Su, Q., 2021. Pathophysiological communication between hepatocytes and non-parenchymal cells in liver injury from NAFLD to liver fibrosis. Adv. Drug. Deliv. Rev. 176, 113869.

Lang, Z., Yu, S., Hu, Y., Tao, Q., Zhang, J., Wang, H., Zheng, L., Yu, Z., Zheng, J., 2023. Ginsenoside Rh2 promotes hepatic stellate cell ferroptosis and inactivation via regulation of IRF1-inhibited SLC7A11. Phytomedicine 118, 154950.

Leonard, S., Wei, W., Anderton, J., Vockerodt, M., Rowe, M., Murray, P.G., Woodman, C. B., 2011. Epigenetic and transcriptional changes which follow Epstein-Barr virus infection of germinal center B cells and their relevance to the pathogenesis of Hodgkin's lymphoma. J. Virol. 85, 9568–9577.

Li, J., Cao, F., Yin, H.L., Huang, Z.J., Lin, Z.T., Mao, N., Sun, B., Wang, G., 2020a. Ferroptosis: past, present and future. Cell Death. Dis. 11, 88.

Li, L., Wang, K., Jia, R., Xie, J., Ma, L., Hao, Z., Zhang, W., Mo, J., Ren, F., 2022. Ferroportin-dependent ferroptosis induced by ellagic acid retards liver fibrosis by impairing the SNARE complexes formation. Redox Biol. 56, 102435.

Li, W., Wang, J.Q., Zhou, Y.D., Hou, J.G., Liu, Y., Wang, Y.P., Gong, X.J., Lin, X.H., Jiang, S., Wang, Z., 2020b. Rare ginsenoside 20(R)-Rg3 inhibits D-galactose-induced Liver and kidney injury by regulating oxidative stress-induced apoptosis. Am. J. Chin. Med. 48, 1141–1157.

Liao, P., Wang, W., Wang, W., Kryczek, I., Li, X., Bian, Y., Sell, A., Wei, S., Grove, S., Johnson, J.K., Kennedy, P.D., Gijón, M., Shah, Y.M., Zou, W., 2022. CD8(+) T cells and fatty acids orchestrate tumor ferroptosis and immunity via ACSL4. Cancer Cell 40, 365–378 e366.

Liu, X., Mi, X., Wang, Z., Zhang, M., Hou, J., Jiang, S., Wang, Y., Chen, C., Li, W., 2020. Ginsenoside Rg3 promotes regression from hepatic fibrosis through reducing inflammation-mediated autophagy signaling pathway. Cell Death. Dis. 11, 454.

Luo, P., Liu, D., Zhang, Q., Yang, F., Wong, Y.K., Xia, F., Zhang, J., Chen, J., Tian, Y., Yang, C., Dai, L., Shen, H.M., Wang, J., 2022. Celastrol induces ferroptosis in activated HSCs to ameliorate hepatic fibrosis via targeting peroxiredoxins and HO-1. Acta Pharm. Sin. B 12, 2300–2314.

Luo, Y., Huang, Q., He, B., Liu, Y., Huang, S., Xiao, J., 2021. Regulation of ferroptosis by non-coding RNAs in the development and treatment of cancer (review). Oncol. Rep. 45, 29–48.

Miao, Z., Tian, W., Ye, Y., Gu, W., Bao, Z., Xu, L., Sun, G., Li, C., Tu, Y., Chao, H., Lam, S. M., Liu, N., Ji, J., 2022. Hsp90 induces Acsl4-dependent glioma ferroptosis via dephosphorylating Ser637 at Drp1. Cell Death. Dis. 13, 548.

Parola, M., Pinzani, M., 2019. Liver fibrosis: pathophysiology, pathogenetic targets and clinical issues. Mol. Aspects Med. 65, 37–55.

Peng, X., Wu, X., Wu, G., Peng, C., Huang, B., Huang, M., Ding, J., Mao, C., Zhang, H., 2023. MiR-129-2-3p inhibits esophageal carcinoma cell proliferation, migration, and invasion via targeting DNMT3B. Curr. Mol. Pharmacol. 16, 116–123.

Shan, X., Tian, L.L., Zhang, Y.M., Wang, X.Q., Yan, Q., Liu, J.W., 2015. Ginsenoside Rg3 suppresses FUT4 expression through inhibiting NF-κB/p65 signaling pathway to promote melanoma cell death. Int. J. Oncol. 47, 701–709.

Stockwell, B.R., Friedmann Angeli, J.P., Bayir, H., Bush, A.I., Conrad, M., Dixon, S.J., Fulda, S., Gascón, S., Hatzios, S.K., Kagan, V.E., Noel, K., Jiang, X., Linkermann, A., Murphy, M.E., Overholtzer, M., Oyagi, A., Pagnussat, G.C., Park, J., Ran, Q., Rosenfeld, C.S., Salnikow, K., Tang, D., Torti, F.M., Torti, S.V., Toyokuni, S., Woerpel, K.A., Zhang, D.D., 2017. Ferroptosis: a regulated cell death nexus linking metabolism. Redox Biol. Dis. Cell 171, 273–285.

Teng, S., Wang, Y., Li, P., Liu, J., Wei, A., Wang, H., Meng, X., Pan, D., Zhang, X., 2017. Effects of R type and S type ginsenoside Rg3 on DNA methylation in human hepatocarcinoma cells. Mol. Med. Rep. 15, 2029–2038.

Veland, N., Hardikar, S., Zhong, Y., Gayatri, S., Dan, J., Strahl, B.D., Rothbart, S.B., Bedford, M.T., Chen, T., 2017. The arginine methyltransferase PRMT6 regulates DNA methylation and contributes to global DNA hypomethylation in cancer. Cell Rep. 21, 3390–3397.

Vrtačnik, P., Marc, J., Ostanek, B., 2015. Hypoxia mimetic deferoxamine influences the expression of histone acetylation- and DNA methylation-associated genes in osteoblasts. Connect. Tissue Res. 56, 228–235.

Wang, Q., Zhang, F., Lei, Y., Liu, P., Liu, C., Tao, Y., 2021. microRNA-322/424 promotes liver fibrosis by regulating angiogenesis through targeting CUL2/HIF-1α pathway. Life Sci. 266, 118819.

Wang, T.X., Liang, J.Y., Zhang, C., Xiong, Y., Guan, K.L., Yuan, H.X., 2019. The oncometabolite 2-hydroxyglutarate produced by mutant IDH1 sensitizes cells to ferroptosis. Cell Death Dis. 10, 755.

Wang, Y., Zhang, M., Bi, R., Su, Y., Quan, F., Lin, Y., Yue, C., Cui, X., Zhao, Q., Liu, S., Yang, Y., Zhang, D., Cao, Q., Gao, X., 2022. ACSL4 deficiency confers protection against ferroptosis-mediated acute kidney injury. Redox Biol. 51, 102262.

Wu, J., Zhang, R., Shen, F., Yang, R., Zhou, D., Cao, H., Chen, G., Pan, Q., Fan, J., 2018a. Altered DNA methylation sites in peripheral blood leukocytes from patients with simple steatosis and nonalcoholic steatohepatitis (NASH). Med. Sci. Monit. 24, 6946–6967.

Wu, X., Zhi, F., Lun, W., Deng, Q., Zhang, W., 2018b. Baicalin inhibits PDGF-BB-induced hepatic stellate cell proliferation, apoptosis, invasion, migration and activation via the miR-3595/ACSL4 axis. Int. J. Mol. Med. 41, 1992–2002.

Xia, J., Ma, S., Zhu, X., Chen, C., Zhang, R., Cao, Z., Chen, X., Zhang, L., Zhu, Y., Zhang, S., Li, S., Gu, G., Wei, X., Yu, K., Wang, J., 2022. Versatile ginsenoside Rg3 liposomes inhibit tumor metastasis by capturing circulating tumor cells and destroying metastatic niches. Sci. Adv. 8, eabj1262.

Yi, J., Wu, S., Tan, S., Qin, Y., Wang, X., Jiang, J., Liu, H., Wu, B., 2021. Berberine alleviates liver fibrosis through inducing ferrous redox to activate ROS-mediated hepatic stellate cells ferroptosis. Cell Death Discov. 7, 374.

Yu, F., Chen, B., Dong, P., Zheng, J., 2020. HOTAIR epigenetically modulates PTEN expression via microRNA-29b: a novel mechanism in regulation of liver fibrosis. Mol. Ther. 28, 2703.
Yu, F., Geng, W., Dong, P., Huang, Z., Zheng, J., 2018. LncRNA-MEG3 inhibits activation of hepatic stellate cells through SMO protein and miR-212. Cell Death Dis. 9, 1014.
Yuan, S., Wei, C., Liu, G., Zhang, L., Li, J., Li, L., Cai, S., Fang, L., 2022. Sorafenib attenuates liver fibrosis by triggering hepatic stellate cell ferroptosis via HIF-1α/SLC7A11 pathway. Cell Prolif. 55, e13158.
Yue, Z., Jiang, Z., Ruan, B., Duan, J., Song, P., Liu, J., Han, H., Wang, L., 2021. Disruption of myofibroblastic Notch signaling attenuates liver fibrosis by modulating fibrosis progression and regression. Int. J. Biol. Sci. 17, 2135–2146.
Zhang, K., Chang, Y., Shi, Z., Han, X., Han, Y., Yao, Q., Hu, Z., Cui, H., Zheng, L., Han, T., Hong, W., 2016. ω-3 PUFAs ameliorate liver fibrosis and inhibit hepatic stellate cells proliferation and activation by promoting YAP/TAZ degradation. Sci. Rep. 6, 30029.
Zhang, L., Liao, Y., Tang, L., 2019. MicroRNA-34 family: a potential tumor suppressor and therapeutic candidate in cancer. J. Exp. Clin. Cancer Res. 38, 53.
Zhang, M., Gao, Y., Li, Q., Cao, H., Yang, J., Cai, X., Xiao, J., 2022. Downregulation of DNA methyltransferase-3a ameliorates the osteogenic differentiation ability of adipose-derived stem cells in diabetic osteoporosis via Wnt/β-catenin signaling pathway. Stem Cell Res. Ther. 13, 397.
Zhang, R.N., Pan, Q., Zheng, R.D., Mi, Y.Q., Shen, F., Zhou, D., Chen, G.Y., Zhu, C.Y., Fan, J.G., 2018. Genome-wide analysis of DNA methylation in human peripheral leukocytes identifies potential biomarkers of nonalcoholic fatty liver disease. Int. J. Mol. Med. 42, 443–452.
Zhang, Z., Guo, M., Shen, M., Kong, D., Zhang, F., Shao, J., Tan, S., Wang, S., Chen, A., Cao, P., Zheng, S., 2020. The BRD7-P53-SLC25A28 axis regulates ferroptosis in hepatic stellate cells. Redox. Biol. 36, 101619.
Zhou, G., Li, C., Zhan, Y., Zhang, R., Lv, B., Geng, W., Zheng, J., 2020. Pinostilbene hydrate suppresses hepatic stellate cell activation via inhibition of miR-17-5p-mediated Wnt/β-catenin pathway. Phytomedicine 79, 153321.